Chinese Journal of Natural Medicines

# Nuciferine ameliorates cognitive impairment and insulin resistance in T2DM by targeting the insulin receptor and activating PI3K/AKT signaling

Miao Zheng, Can Wang, Jiayi Liu, Yi Xia, Xinyue Zhang, Lili Gu

**Citation:** Miao Zheng, Can Wang, Jiayi Liu, Yi Xia, Xinyue Zhang, Lili Gu, Nuciferine ameliorates cognitive impairment and insulin resistance in T2DM by targeting the insulin receptor and activating PI3K/AKT signaling, Chinese Journal of Natural Medicines, 2026, 24(7), 819−831. doi: 10.1016/S1875−5364(26)61190−9.

View online: https://doi.org/10.1016/S1875−5364(26)61190−9

## Related articles that may interest you

20(*S*)−ginsenoside Rh1 alleviates T2DM induced liver injury *via* the Akt/FOXO1 pathway

Chinese Journal of Natural Medicines. 2022, 20(9), 669−678 https://doi.org/10.1016/S1875−5364(22)60201−2

Effective fraction from Simiao Wan prevents hepatic insulin resistant by inhibition of lipolysis *via* AMPK activation

Chinese Journal of Natural Medicines. 2022, 20(3), 161−176 https://doi.org/10.1016/S1875−5364(21)60115−2

*Jiedu Sangen* decoction inhibits chemoresistance to 5−fluorouracil of colorectal cancer cells by suppressing glycolysis *via* PI3K/AKT/HIF−1 $\alpha$ signaling pathway

Chinese Journal of Natural Medicines. 2021, 19(2), 143−152 https://doi.org/10.1016/S1875−5364(21)60015−8

Gualou−Xiebai−Banxia decoction protects against type II diabetes with acute myocardial ischemia by attenuating oxidative stress and apoptosis *via* PI3K/Akt/eNOS signaling

Chinese Journal of Natural Medicines. 2021, 19(3), 161−169 https://doi.org/10.1016/S1875−5364(21)60017−1

Seed oil of *Brucea javanica* induces apoptosis through the PI3K/Akt signaling pathway in acute lymphocytic leukemia Jurkat cells

Chinese Journal of Natural Medicines. 2021, 19(8), 608−620 https://doi.org/10.1016/S1875−5364(21)60060−2

The bioinformatics and metabolomics research on anti−hypoxic molecular mechanisms of Salidroside *via* regulating the PTEN mediated PI3K/Akt/NF− $\kappa$ B signaling pathway

Chinese Journal of Natural Medicines. 2021, 19(6), 442−453 https://doi.org/10.1016/S1875−5364(21)60043−2

Wechat

Chinese Journal of Natural Medicines 24 (2026) 819-831

Contents lists available at ScienceDirect

Chinese Journal of Natural Medicines

journal homepage: www.cjnmcpu.com/



Original article

# Nuciferine ameliorates cognitive impairment and insulin resistance in T2DM by targeting the insulin receptor and activating PI3K/AKT signaling

Miao Zheng, Can Wang, Jiayi Liu, Yi Xia, Xinyue Zhang*, Lili Gu*

*School of Pharmacy, Hangzhou Medical College, Hangzhou 310013, China*

ARTICLE INFO

*Article history:*
Received 1 July 2025
Revised 11 September 2025
Accepted 29 November 2025
Available online 20 July 2026

*Keywords:*
Nuciferine
T2DM-CI
PI3K/AKT pathway
Insulin receptor
Neuroprotection
Insulin resistance

ABSTRACT

Insulin resistance is a hallmark of type 2 diabetes (T2DM) and can increase the risk of cognitive impairment, including Alzheimer's disease. Nuciferine, an alkaloid derived from lotus leaves, shows neuroprotective effects. This study investigated nuciferine's protective role in T2DM-induced cognitive impairment (T2DM-CI) and its mechanisms. Mouse models were created using high-fat diets and streptozotocin, along with high glucose-induced HT-22 cells. Nuciferine reduced blood glucose, improved cognitive function, and mitigated glial cell activation, neuron and synapse loss in T2DM mice. It enhanced insulin signaling by increasing protein levels of IR, IRS1, and IGF-1R, reversing PI3K and AKT phosphorylation, inhibiting GSK3β activity, and reducing hyperphosphorylated Tau in HT-22 cells and T2DM mice. mRNA levels of these molecules matched their protein levels. Further studies revealed that nuciferine directly interacts with IR, knocking out IR abolished its effects on the PI3K/AKT pathway. Thus, nuciferine activates the PI3K/AKT pathway *via* IR, improving insulin resistance and slowing T2DM-CI progression.

## 1. Introduction

Type 2 diabetes mellitus (T2DM) is characterized by hyperglycemia and insulin resistance [1], leading to diverse complications such as neuropathy [2], diabetic retinopathy [3], diabetic kidney disease [4] and coronary artery disease [5]. According to the International Diabetes Federation (IDF), the global prevalence of diabetes has surpassed 828 million individuals, with projections indicating a rise to 1.3 billion by 2050 [6]. Alzheimer's disease (AD) is a neurodegenerative disorder marked by progressive cognitive decline and characterized by amyloid-β (Aβ) plaques and hyperphosphorylated Tau neurofibrillary tangles [7]. Global dementia cases reached 57.4 million in 2019, with AD representing 60%–80% of these cases [8]. Epidemiological evidence indicates that T2DM patients have a 1.5 to 2.5-fold higher risk of cognitive decline progressing from mild impairment to AD compared to non-diabetics [9]. Preclinical investigations reveal that streptozotocin (STZ)-induced diabetic rats exhibit cerebral aging and AD-like changes [10]. Due to the complex causes of T2DM-induced cognitive impairment (T2DM-CI) and lack of effective treatments, understanding its mechanisms is critical to developing targeted strategies.

Insulin resistance plays a pivotal role in the progression of T2DM [1] and is closely associated with the pathological mechanisms underlying cognitive impairment [11]. Insulin resistance disrupts glucose utilization in the central nervous system, thereby impairing synaptic plasticity and affecting learning and memory functions [12]. Furthermore, insulin signaling exerts a pivotal function in inhibiting the aberrant activation of glycogen synthase kinase-3β (GSK3β) [13]. This inhibition effectively prevents Tau protein hyperphosphorylation, and the formation of neurofibrillary tangles (NFTs), thus mitigating neurotoxicity. The insulin signaling pathway includes the phosphoinositide 3-kinase (PI3K)/protein kinase B (AKT) and mitogen-activated protein kinase/extracellular signal-regulated kinase (MAPK/MEK) pathways, with PI3K/AKT being the most important [14]. In AD patients, impaired insulin signaling inhibits PI3K/AKT, activating GSK3β and causing glucose metabolism disorders, Tau hyperphosphorylation, and neuronal death, which drives AD progression [15]. Thus, the PI3K/AKT pathway may be key to treating T2DM-CI.

*Nelumbo nucifera* Gaertn. has been served as food in China for millennia. Its seeds, plumule, and leaves are used in traditional Chinese medicine (TCM) to treat fever, diarrhea, and bleeding [16]. Nuciferine (Fig. 1A), an alkaloid bearing an aromatic ring, is the principal bioactive constituent obtained from lotus leaf (*N. nucifera* leaves) and has a broad spectrum of pharmacological activities [17]. Nuciferine shows promise in managing diabetes by restoring impaired glucose tolerance and insulin resistance [18], and improving fatty acid accumulation and ferroptosis [19, 20]. Li et al. [21] found that nuciferine attenuates neuroinflammation associated with cerebral ischemia-reperfusion injury. Besides, Chen et al. [22] found nuciferine can exert a protective effect on brain injury by regulating lipid metabolism (including arachidonic acid metabolism, sphingolipid metabolism). Therefore, nuciferine not only exhibits the effect of reducing blood sugar but also provides protection against brain damage. Nevertheless, whether nuciferine has therapeutic effects on T2DM-CI has not yet been reported.

In this study, we developed *in vivo* models that included a high-fat diet (HFD) combined with streptozotocin (STZ) adminis-

* Corresponding author.
*E-mail addresses:* 2020000331@hmc.edu.cn (X. Zhang); 2020000292@hmc.edu.cn (L. Gu)

https://doi.org/10.1016/S1875-5364(26)61190-9
Copyright © 2026, China Pharmaceutical University. Published by Elsevier B.V. All rights are reserved.

tration and intracerebroventricular (ICV) injection of STZ. Furthermore, an *in vitro* model was established by culturing HT-22 cells under high-glucose (HG) stimulation conditions. Nuciferine treatment significantly reduced blood glucose, alleviated cognitive dysfunction, mitigated glial cell activation, neuronal loss, and synaptic degeneration in mice. It enhanced the expression of insulin-related signaling molecules like insulin receptor (IR), insulin receptor substrate 1 (IRS1), and insulin-like growth factor 1 receptor (IGF-1R), reversed the phosphorylation levels of PI3K and AKT, inhibited GSK3β activity, and decreased hyperphosphorylation Tau protein levels both *in vivo* and *in vitro*. Nuciferine was found to interact directly with IR. Once IR was knocked out, the interaction nullified the regulatory effects of nuciferine on the PI3K/AKT pathway. The results of this study highlight the promise of nuciferine in improving insulin resistance and mitigating the progression of T2DM-CI by targeting IR.

## 2. Materials and methods

### 2.1. Reagents

Nuciferine (98% purity, PRF21110246) and Metformin (98% purity, ACG4579) were purchased from Biopurify Phytochemicals Ltd. (Chengdu, China) and MERCK (Jiangsu, China), respectively. STZ (98% purity,S817944), LY294002 (98% purity, L832989), and BMS-754807 (98% purity, B87322) were purchased from Macklin(Shanghai, China), while HG (99.8% purity, No. 2230821002) was purchased from Solarbio (Beijing, China) and the DCFH-DA reagent (S0033S) from Beyotime (Shanghai, China). DMEM was acquired from Gibco (USA).

### 2.2. Animals group and treatments

Male C57BL/6J mice (8 weeks old, weight 20 ± 2 g) were provided by the Laboratory Animal Center of Hangzhou Medical College (Certificate No. 20221214Abzz0100018959). The mice were maintained in a standard laboratory with 55% ± 5% humidity, a temperature of 25 ± 1 °C, and a 12-h light/dark cycle. All experiments were approved by the Zhejiang Provincial Laboratory Animal Welfare and Ethics Committee (Approval No. ZJCLA-IACUC-20010127).

HFD/STZ mice were divided into a normal diet group and an HFD group after a 7-day adaptation period. Mice in the normal diet group were fed a regular diet, while those in the HFD group were fed a high-fat diet for 4 consecutive weeks to induce insulin resistance. All mice were then fasted for 12 h and received intraperitoneal injections of 60 mg·kg$^{-1}$ STZ in 0.5 mol·L$^{-1}$ sodium

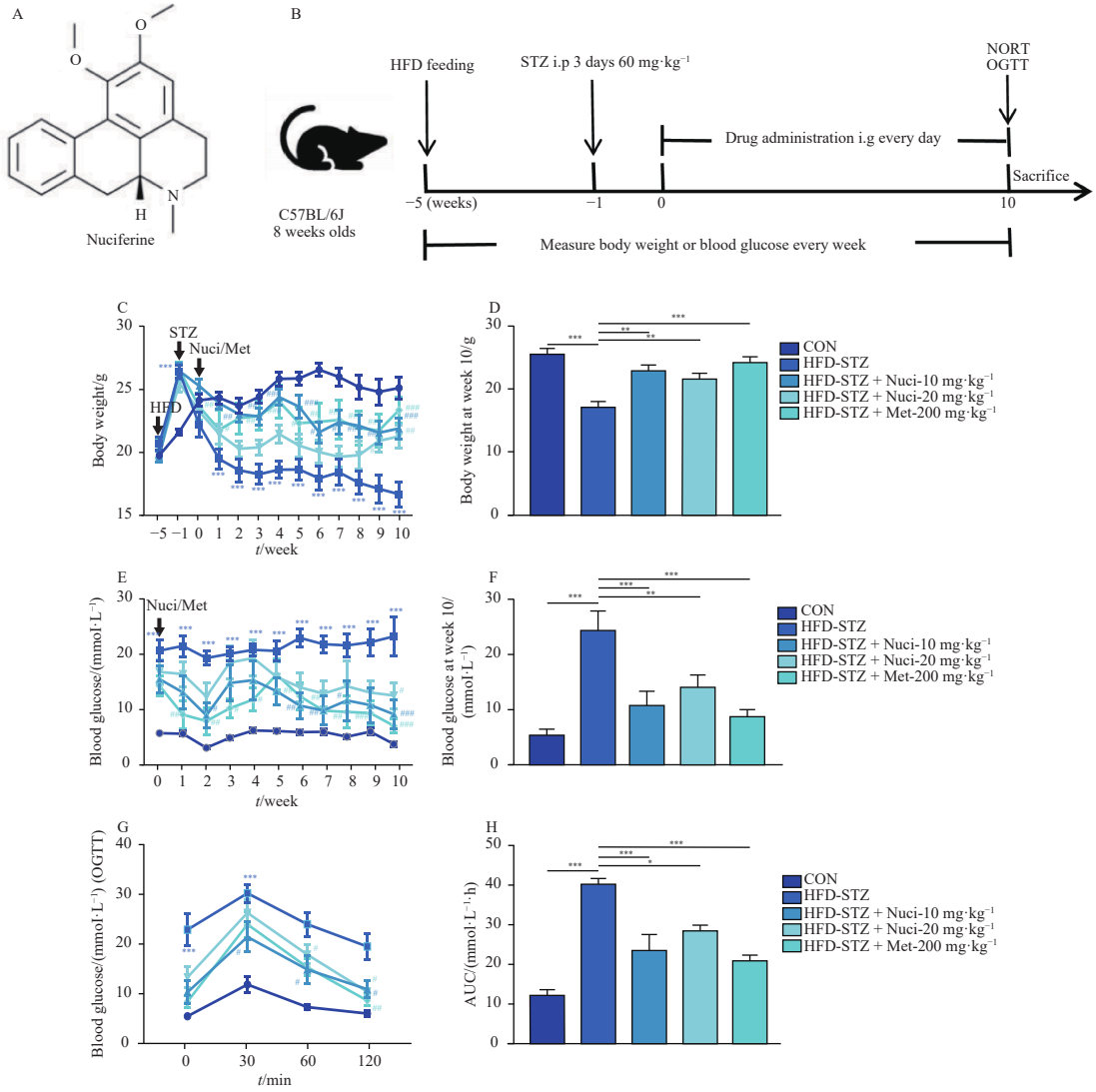



**Fig. 1** Nuciferine enhanced body weight and mitigated blood glucose in HFD/STZ-induced mice. (A) Chemical structure of nuciferine. (B) Animal experimentation process. (C and D) Changes in body weight and weight since last dosing (week 10). (E and F) Changes in blood glucose levels and blood glucose since last dosing (week 10). (G) Oral glucose tolerance test (OGTT). (H) Area under curve (AUC) of OGTT. Data were expressed as mean ± SEM ($n$ = 8–10). $^{*}P < 0.05$, $^{**}P < 0.01$, $^{***}P < 0.001$.

citrate buffer for 3 consecutive days. One week after injection, mice with blood glucose levels higher than 11.1 mmol·L$^{-1}$ were classified as T2DM mice. Subsequently, the mice were randomly divided into 5 groups ($n$ = 10 in each group): control group (CON), model group (HFD-STZ), low-dose nuciferine group (Nuci-10 mg·kg$^{-1}$), high-dose nuciferine group (Nuci-20 mg·kg$^{-1}$), and metformin positive group (Met-200 mg·kg$^{-1}$). From the 6$^{th}$ week, treatment groups received daily intragastric nuciferine or metformin for 10 weeks as in Fig. 1B. The body weight and fasting blood glucose were monitored weekly. In the 10$^{th}$ week, OGTT and NOR tests were done to assess metabolic and cognitive effects.

Following a 7-day adaptation period, ICV/STZ mice were divided into a control group and a modeling group. Mice in the modeling group received an intracerebroventricular injection of STZ (3 mg·kg$^{-1}$) to establish an insulin resistance model, whereas those in the control group received intracerebroventricular injection of citrate buffer. One week after injection, all mice were randomly assigned to five groups ($n$ = 10 in each group): control group (CON), model group (ICV-STZ), low-dose nuciferine group (Nuci-20 mg·kg$^{-1}$), high-dose nuciferine group (Nuci-40 mg·kg$^{-1}$), and donepezil (Don-1.5 mg·kg$^{-1}$). Beginning in the 2$^{nd}$ week, mice in the treatment groups received daily intragastric nuciferine or donepezil for 4 weeks as illustrated in Fig. S5A. During the 4$^{th}$ week, MWM test was performed to assess cognitive effects.

### 2.3. Novel object recognition (NOR) test

The NOR test was conducted to further evaluate the cognitive function of mice after drug intervention. The experiment was conducted in a 50 cm square test box with symmetrical exploration areas, a camera, and lighting. It consisted of two phases: familiarization and testing. In the familiarization phase, mice explored two identical objects for 5 min. After 24 h, one object was replaced with a new one of different shape and color for the testing phase. Mice were placed in the box facing away from the objects and allowed to explore freely for 5 min. Data were recorded using Tracking Master V4.1.0 software. The discrimination index (DI) was calculated as: (time exploring new object/total exploration time) × 100%.

### 2.4. Morris water maze (MWM) test

The MWM test was conducted to evaluate the cognitive function of mice after drug intervention. The experiment used a 1.2 m-diameter, 0.6 m-deep pool with a 5 cm-diameter escape platform and a camera for recording mouse behavior. During the training phase (days 1–5), mice were tested four times daily from different quadrants. Finding the platform was recorded for up to 60 sec per trial. If the platform was found within 5 sec, recording stopped; otherwise, mice were guided to the platform and allowed to stay for 15 sec to reinforce memory. On the test day (day 6), the platform was removed, and the number of crossings over the original platform area within 60 sec was recorded. Data were analyzed using Tracking Master V4.1.0 software.

### 2.5. Oral glucose tolerance test (OGTT)

After the administration was completed, the mice were fasted for 12 h without water restriction and then orally administered 1.8 g·kg$^{-1}$ of glucose. Blood samples were collected at different time points of 0, 30, 60 and 120 min to measure blood glucose. The data were recorded to draw the glucose tolerance curve and calculate the area under the curve (AUC).

### 2.6. Hematoxylin eosin (HE) staining

The brain tissue was subjected to fixation, dehydration, embedding, sectioning, and dewaxing. It was stained with hematoxylin for 3 min and rinsed with distilled water. Subsequently, differentiation was carried out using 10% hydrochloric acid ethanol for 5 sec, and then the sections were re-blued with lithium carbonate. Eosin staining persisted for 2 min before dehydration in ethanol and two rounds of xylene-based clearing for 10 min each. Eventually, the sections were mounted with neutral tree gum. The pathological features of the hippocampus were observed under a microscope.

### 2.7. Immunofluorescence (IF)

The brains of mice were fixed in 4% paraformaldehyde (BL539A, Biosharp,Guangzhou, China) for 24 h and washed with PBS. Tissue permeabilization was done with 0.3% Triton X-100, and non-specific binding sites were blocked with 5% fetal bovine serum(40130ES76,Yeasen,Shanghai,China) at room temperature for 30 min. After discarding the blocking solution, diluted primary antibodies, containing Tau (1∶200, ab32057, abcam, USA), SYP (1∶800, 17785-1-AP, Proteintech), NeuN (1∶500, 26975-1-AP, Proteintech) were added and incubated overnight at 4 °C. Extensive washing was done before adding a fluorescently labeled secondary antibody, which was incubated at room temperature in the dark for 2 h. After more washes and removing the secondary antibody working solution, the nuclei were stained with DAPI. Immunofluorescence images were captured and analyzed using ImageJ software (NIH,Bethesda,MD,USA) to quantify the mean optical density values.

### 2.8. Proteomic analysis

The total proteins in mouse brain tissues were extracted and quantified by the BCA method. After SDS-PAGE electrophoresis, proteolysis, peptide desalting and quantification, DIA mass spectrometry was done. The SpectronautTM18 software built a mouse protein database, Bioinformatics analysis was conducted on the cloud platform (cloud.majorbio.com). $P$ values and fold change (FC) between groups were calculated using R' $t$-test function. Differentially expressed proteins (DEPs) were defined as those with $P$ < 0.05 and an absolute FC > 1.1. Gene Ontology (GO) annotation of DEPs was performed from three aspects using the GO database (http://geneontology.org/). The Kyoto Encyclopedia of Genes and Genomes (KEGG) database (https://www.genome.jp/kegg/) was utilized to analyze metabolic pathways. The proteomic analysis was by Applied Protein Technology Co., Ltd. (Shanghai, China).

### 2.9. Cell culture

The HT-22 cell line was obtained from Nanjing Shenghang Biotechnology Co., Ltd. (Nanjing, China). The cells were grown in high-glucose DMEM with 10% FBS, 100 U·mL$^{-1}$ penicillin and 100 μg·mL$^{-1}$ streptomycin at 37 °C in a 5% $CO_2$ atmosphere. The culture medium was changed every 1–2 days, and the passage number of cells used in all experiments was between 5 and 15.

### 2.10. MTT assay

The HT-22 cells cultured to the logarithmic growth phase were digested into cell suspensions and inoculated into 96-well plates. When the cell density reached 50%–60%, the cells were preincubated with different concentrations of nuciferine for 4 h, and then, except for the normal group, all groups were treated with HG for 24 h to determine the cell viability. Cell viability was determined by the MTT assay. After the cell treatment, 20 μL of MTT was added to the cells, and after 4 h of incubation, 150 μL of DMSO (ST038-500 ml, Beyotime, Shanghai, China) was added to each well. Finally, the absorbance was measured at a wavelength

of 570 nm using a microplate reader (BioTek Cytation 1, USA).

### 2.11. Reactive oxygen species (ROS) staining

HT-22 cells were plated in 6-well plates at a density of 40 × $10^4$ cells per well. After drug treatment, the DCFH-DA probe was diluted 1∶1000 in serum-free DMEM, and 1 mL was added to each well. The cells were incubated at 37 °C with 5% $CO_2$ for 30 min in the dark. Then, the cells were washed twice with serum-free DMEM to remove the excessive probe. The fluorescence intensity was measured by a microplate reader and analyzed with ImageJ software. Green fluorescence intensity indicated the intracellular ROS levels.

### 2.12. Western blotting

Protein lysates were made with RIPA buffer, and protein concentrations were measured by the BCA assay. The proteins were denatured at 95 °C for 5 min, separated by electrophoresis on a 10% SDS-PAGE gel (BRK0003-125T, ABclonal, Wuhan, China), and electrotransferred to a PVDF (IPVH00010, MercK Milipore, Darmstadt, Germany) membrane. The membrane was blocked with 5% non-fat milk in TBST for 2 h at room temperature and incubated with primary antibodies, including IDE (1∶5000, ab109538, abcam, USA), NEP (1∶5000, ab256494, abcam, USA), Tau (1∶1000), p-Tau (1∶2000, ab109390, abcam, USA), IRS1 (1∶1000, 2382S, CST, USA), p-IRS1 (Ser636/639) (1∶1000, 2388S, CST, USA), PI3K (1∶1000, 4292S; CST; USA), p-PI3K (Tyr458) (1∶1000, 4228T, CST, USA), AKT (1∶1000, 9272S, CST, USA), p-AKT (1∶1000, 9271T, CST, USA), IGF-1R (1∶1000, 3027S, CST, USA), p-IGF-1R (Tyr1135/1136) (1∶1000, 3024S, CST, USA), IR (1∶1000, 3025S, CST, USA), GSK3β (1∶1000, AF5016, Affinity, USA ), p-GSK3β (1∶1000, AF3335, Affinity, USA), GAPDH (1∶5000, FD0063, Fudebio, China) overnight at 4 °C. After washing with 1 × TBST, the membrane was exposed to the secondary antibody for 1 h at room temperature. Chemiluminescent detection was done using NcmECL Ultra (AP34L025, LIFE-iLAB, Shanghai, China) and visualized with an Amersham ImageQuant 800 system (Cytiva, Marlborough, MA, USA).

### 2.13. Reverse transcription-quantitative PCR (RT-qPCR)

Total RNA was extracted by trizol (M1397141, Yeasen, China), and 1 μg total RNA was reverse-transcribed into cDNA using FastKing gDNA Dispelling by Veriti 96-Well Thermal Cycler PCR (Thermo Fisher, 4375786, USA). RT-PCR was performed with Super Real Premix Plus (SybrGreen) (FP205, Tiangan, China) on ABI 7500FastPCR systems (Applied Biosystems, USA). Finally, results were calculated using the $2^{-\Delta\Delta Ct}$ method and mRNA levels were normalized to GAPDH. Primers for RT-PCR are listed in Table S1.

### 2.14. Molecular docking

The 3D structure of nuciferine was retrieved from the PubChem Compound database. The crystal structure of the IR protein was obtained from the RCSB Protein Data Bank, and the PDB files were refined using PyMOL 2.50 (Schrödinger, LLC, NY, USA). Molecular docking simulations were conducted by AutoDock 4.2.6 (Scripps Research, La Jolla, CA, USA), and results with binding affinities less than −5 kJ·$mol^{-1}$ were selected for further analysis. Finally, the binding mode, interaction sites, and binding energy of nuciferine with the IR were visualized using PyMOL 2.50.

### 2.15. Cellular thermal shift assay (CETSA)

HT-22 cells were cultured in 100-mm dishes with high-glucose DMEM until confluence. After trypsinization, PBS washing, and resuspension, the cells underwent three freeze-thaw cycles (30 sec in liquid nitrogen, then room temperature thaw). The suspension was centrifuged at 15 000 × *g* for 20 min at 4 °C. Supernatant was split into two groups (600 μL each): one was treated with 25 μmol·$L^{-1}$ nuciferine, and the other with DMSO as a control. Both groups were incubated at room temperature for 4 h. Samples were aliquoted into six PCR tubes (90 μL each), and subjected to CETSA (40−55 °C, 3 min per step). After heating, samples were transferred to new tubes, centrifuged at 15 000 × *g* for 40 min at 4 °C, after which the supernatants were collected. These were mixed with loading buffer, heated at 95 °C for 5 min, and stored at −80 °C.

### 2.16. siRNA transfection

Before transfection, HT-22 cells were plated in six-well plates and grown for 24 h at 37 °C with 5% $CO_2$. Transfection was done using an siRNA transfection reagent kit (Shanghai Biotend Biotechnology Co., Ltd. (Shanghai, China). IR siRNA and Vehicle siRNA were from Tsingke Biotechnology Co., Ltd. (Hangzhou, China). The siRNA sequences are listed in Table S2.

### 2.17. Statistical analysis

Quantitative data were analyzed using GraphPad Prism 8.0 (GraphPad Software, Inc, USA). Results are expressed as mean ± SEM and presented in graphs. Comparisons between two groups were performed using a *t*-test, and one-way ANOVA was used for multiple-group comparisons. The Bonferroni method was applied for multiple testing correction; $P < 0.05$ was considered statistically significant.

## 3. Results

### 3.1. Nuciferine enhanced body weight and mitigated blood glucose in T2DM mice

As shown in Figs. 1C and 1D, mice fed a HFD for 4 weeks weighed significantly more than the CON group. After 3 days of STZ injection, the weight of the HFD/STZ group dropped after one week. In contrast, mice treated with nuciferine or metformin had a slower weight decrease and began to gain weight from the $10^{th}$ week.

As shown in Figs. 1E and 1F, the blood glucose levels of mice in the HFD/STZ group were much higher than those in the control group. In contrast, the nuciferine and metformin groups had lower blood glucose levels from week 5. After 10 weeks of treatment, the blood glucose levels of T2DM mice treated with nuciferine or metformin were significantly lower than the HFD/STZ group. Meanwhile, the blood glucose of mice in the control group remained stable.

In the OGTT, all groups of mice reached peak blood glucose 30 min after oral glucose (Fig. 1G). The AUC of the OGTT in each group of mice treated with HFD/STZ was significantly greater than that of the CON group, showing impaired glucose tolerance. After drug treatment, the AUC of OGTT in the Nuci group or the Met group was significantly reduced compared with the HFD/STZ group (Fig. 1H). The above results demonstrate that nuciferine improved weight loss, hypoglycemia and impaired glucose tolerance in T2DM mice.

### 3.2. Nuciferine improved cognitive impairment in T2DM mice

The NOR test was carried out to assess the working memory of mice (Figs. 2A and 2B). The results showed that the DI and the frequency of approaches to novel objects in the HFD/STZ group

was lower than that in the control group. In contrast, nuciferine or metformin treatment groups showed higher DI (Fig. 2C) and the frequency of approaches to novel objects (Fig. 2E) compared with the HFD/STZ group, with no significant difference in average speed among groups (Fig. 2D). These findings suggested that nuciferine enhanced cognitive function in HFD/STZ-induced T2DM mice.

To further confirm that nuciferine enhances learning and memory capabilities, a mouse model was established by ICV/STZ and evaluated through the MWM experiment. The results indicated that nuciferine reduced the escape latency (Fig. S1C), expanded the swimming trajectory (Fig. S1D), increased the number of platform crossings (Fig. S1E), and prolonged the time spent in the target quadrant (Fig. S1G), with no significant difference in average speed among groups (Fig. S1F) in ICV/STZ-induced T2DM mice.

### *3.3. Nuciferine inhibited glial cell activation, promoted neuronal survival and increased the synaptic proteins levels in T2DM mice*

The glial cell activation can trigger neuroinflammation, and the resulting neurofunctional damage plays a significant role in diabetes-related cognitive deficits [23]. In the DG regions of the hippocampus, the HFD/STZ group exhibited a significantly higher number of Iba1$^+$ microglia and GFAP$^+$ astrocytes compared with the CON group. However, these changes were markedly reduced following nuciferine treatment (Figs. 2F–2H).

H&E staining was performed to evaluate the impacts of nuciferine on the neuronal damage induced by HFD/STZ. As depicted in Figs. 3A–3D, neurons in the CON group were intact, featuring round and full nuclei as well as clear boundaries. However, in the HFD/STZ group, the neurons were shrunken and the nuclei were dark-stained. Notably, nuciferine treatment reduced this neuronal damage. Similar improvements were observed in the ICV/STZ mouse model (Fig. S2).

Next, we further inspected neuronal damage and synaptic plasticity with NeuN and SYP. Results showed an increase in NeuN-positive cells after nuciferine treatment in the CA1 region of the hippocampus (Figs. 3E and 3F). The HFD/STZ group exhibited a significantly lower intensity of SYP in the CA3 region compared to the control group. However, nuciferine treatment effectively attenuated this reduction (Figs. 3E and 3G). These findings suggested that nuciferine mitigated the impairment of hippocampal neurons in T2DM mice induced by HFD/STZ.

### *3.4. Nuciferine attenuated Tau hyperphosphorylation and enhanced the expression of Aβ-degrading enzymes in T2DM mice*

During T2DM-induced cognitive impairment, brain pathological changes resemble the hyperphosphorylated Tau accumulation observed in AD. As expected, nuciferine-treated mice exhibited reduced Tau levels than HFD/STZ mice (Figs. 4A and 4B), and Tau phosphorylation was also decreased (Figs. 4C and 4F). We further determined the levels of Aβ-degrading enzymes (IDE and NEP) in the hippocampus. Results indicated that nuciferine treatment significantly upregulated IDE and NEP expression in comparison to the HFD/STZ group (Figs. 4C–4E). Similar effects were observed in the ICV/STZ mouse model, where nuciferine treatment led to a significant increase in IDE and NEP expression (Figs. S3A and S3B) and a reduction in the hippocampal p-Tau/Tau ratio(Fig. S3D) compared with the ICV/STZ group.

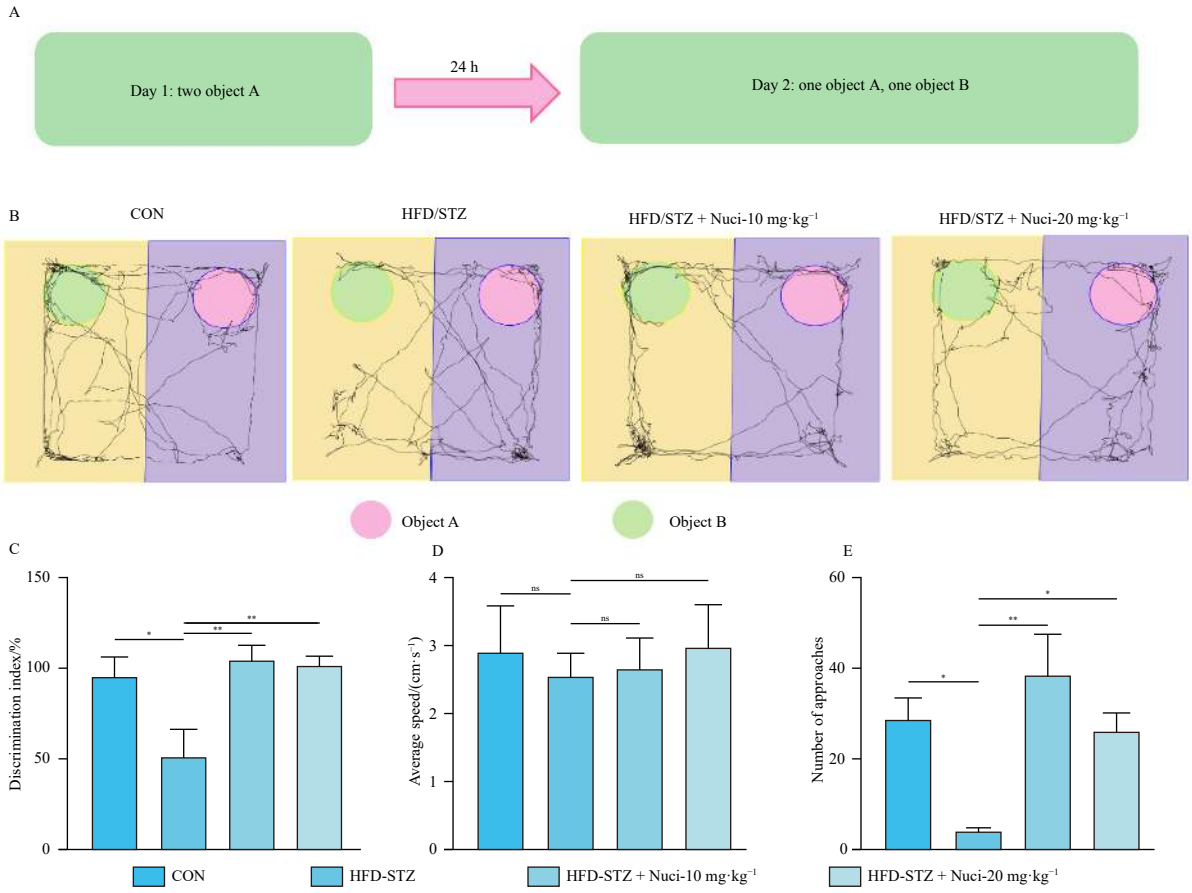



**Fig. 2** Nuciferine alleviated cognitive impairment in HFD/STZ-induced mice. (A) The timeline of the NOR test. (B) The representative trajectory from the NOR experiment. (C) The discrimination index on the 2$^{th}$ day of the NOR test. (D) The average speed during the NOR test on the 2$^{th}$ day. (E) The number of novel object approaches on the 2$^{th}$ day of the NOR test. Data were expressed as mean ± SEM ($n$ = 6). $^{*}P < 0.05$, $^{**}P < 0.01$; ns: no significance.

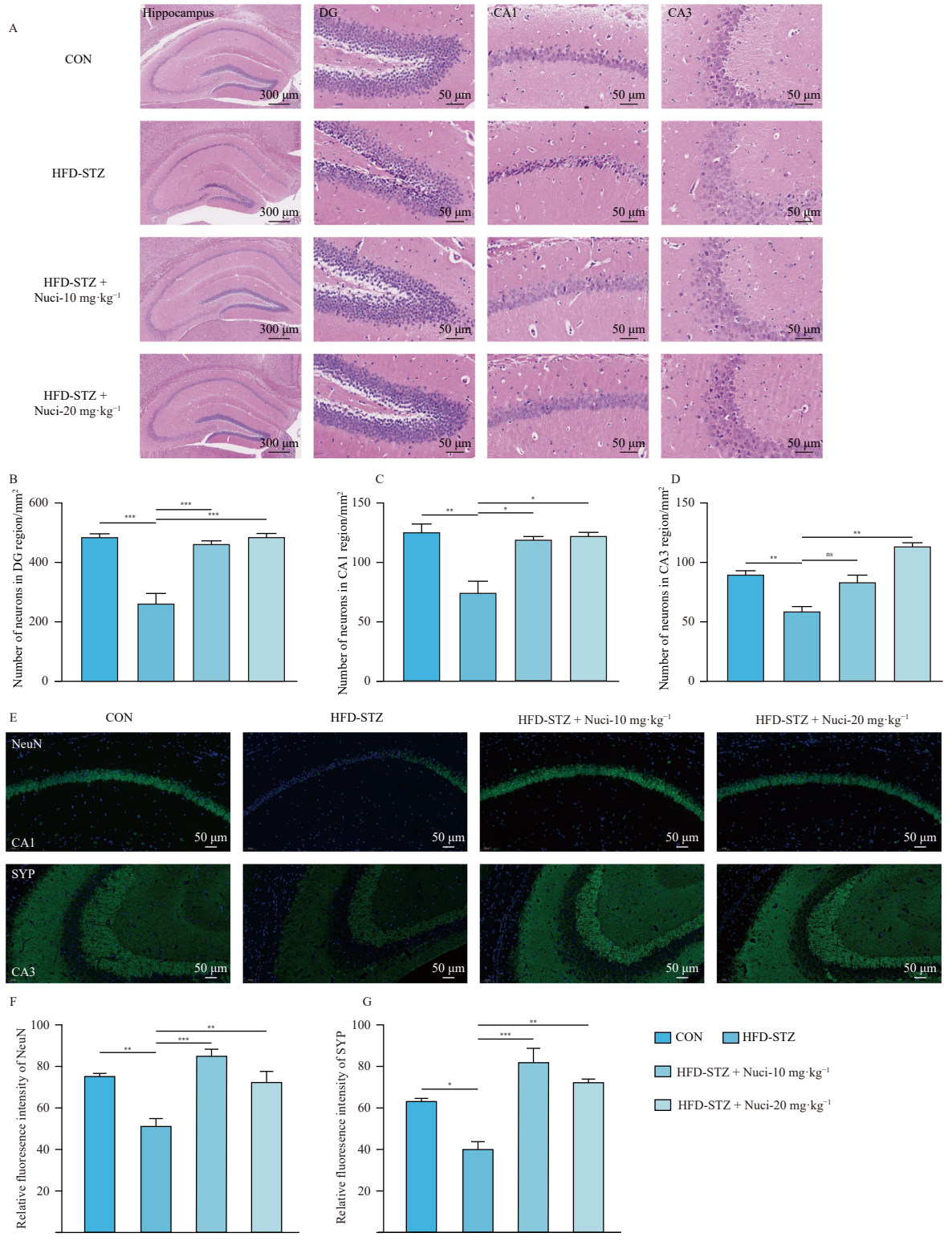



**Fig. 3** Nuciferine enhanced neuronal survival and raised the levels of synaptic proteins in HFD/STZ-induced mice. (A) Representative HE staining images in the hippocampus (scale bar 300 μm) as well as in the DG, CA1, and CA3 regions (scale bar 50 μm). Quantitative analysis of the remaining neurons in the DG (B), CA1 (C), and CA3 (D) regions of the hippocampus. (E) Representative images of NeuN immunofluorescence in CA1 and SYP immunofluorescence in CA3 (scale bar 50 μm). (F) Fluorescence quantification of NeuN from (E). (G) Fluorescence quantification of SYP from (E). Data were expressed as mean ± SEM ($n$ = 3). $^{*}P < 0.05$, $^{**}P < 0.01$, $^{***}P < 0.001$; ns: no significance.

### *3.5. The PI3K/AKT signaling pathway played a critical role in the effect of nuciferine on cognitive impairment in T2DM mice*

Through proteomic analysis, we identified 175 significantly differentially expressed proteins in the Model group compared to the Control group (93 up-regulated and 82 down-regulated) (Fig. S4A). In contrast, the Nuci group showed 158 significantly differentially expressed proteins compared to the Model group (75 up-regulated and 83 down-regulated), as shown in Fig. S4B. Then, GO analysis (Fig. S4C) showed that differentially expressed proteins are enriched in protein kinase binding, neuron projection, signal transduction, intracellular protein transport, signaling receptor binding, translation. KEGG analysis (Fig. 5A) revealed these proteins are concentrated in pathways related to Alzheimer's disease, Type II diabetes mellitus, PI3K/AKT signaling pathway, insulin signaling pathway and neurotrophin signaling

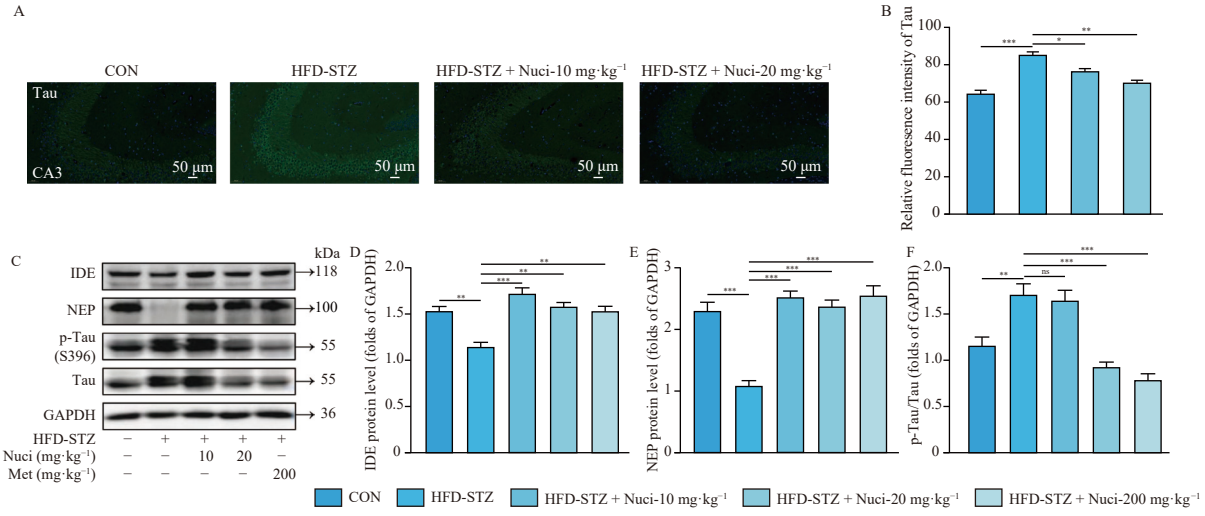



**Fig. 4** Nuciferine enhanced the expression of Aβ-degrading enzymes and alleviated Tau hyperphosphorylation in HFD/STZ-induced mice. (A) Representative images of Tau immunofluorescence in the CA3 regions of the hippocampus (scale bar 50 μm). (B) Quantification of Tau fluorescence from (A). (C) Western blot analysis was conducted for IDE, NEP, p-Tau, and Tau in the hippocampus. (D–F) Quantitative analysis of the blot intensity regarding IDE (D), NEP (E), and the ratio of p-Tau/Tau (F) in panel C. Data were expressed as mean ± SEM ($n$ = 3). $^{**}P < 0.01$, $^{***}P < 0.001$; ns: no significance.

pathway. These results emphasized the connection between insulin resistance and cognitive impairment, with the PI3K/AKT signaling pathway may be a key target for nuciferine's effect onT2DM-CI.

Furthermore, we analyzed the expression of PI3K/AKT pathway-related proteins in mouse hippocampal tissue. In the HFD-STZ model (Figs. 5B–5I), compared to the CON group, the HFD-STZ group showed significantly reduced IR level, the ratios of p-IGF-1R/IGF-1R and p-AKT/AKT, while the ratios of p-IRS1/IRS1 and p-PI3K/PI3K, and GSK3β level was significantly increased. Nuciferine treatment reversed these changes, increasing IR level, the ratio of p-IGF-1R/IGF-1R and p-AKT/AKT while decreasing the ratio of p-IRS1/IRS1, p-PI3K/PI3K, and p-GSK3β/GSK3β. The regulation of the PI3K/AKT pathway by nuciferine was also witnessed in the ICV/STZ mouse model (Fig. S5), where nuciferine treatment enhanced IR level, the ratios of p-IGF-1R/IGF-1R and p-PI3K/PI3K as well as downgraded the ratios of p-IRS1/IRS1 and p-AKT/AKT, and GSK3β level compared with the ICV/STZ group.

### *3.6. Nuciferine alleviated the toxicity and ROS generation in HG-induced HT-22 cells*

To further clarify the improvement effect of nuciferine on T2DM-CI, we established an *in vitro* T2DM model by inducing HT-22 cells with HG. Firstly, we examined the effect of different concentrations of nuciferine on the viability of normal HT-22 cells (Fig. 6A). Within the concentration range of less than 12.5 μmol·L$^{-1}$, nuciferine had no significant effect on the viability of HT-22 cells, confirming this range as safe for subsequent experiments. Next, we explored the effect of different concentrations of HG on the viability of normal HT-22 cells (Fig. 6B). When the HG concentration was 50 mg·mL$^{-1}$, the viability of HT-22 cells was approximately 50%. Thus, we chose HG concentration of 50 mg·mL$^{-1}$ for subsequent modeling experiments. Finally, we assessed nuciferine's ability to improve HT-22 viability after HG treatment (Fig. 6C). Nuciferine treatment increased the viability of HT-22 cells after HG stimulation.

The production of ROS was evaluated by means of DCFH-DA staining. Compared to the CON group, the HG group exhibited a significant increase in ROS fluorescence intensity. In contrast, treatment with both low or high doses of nuciferine reduced ROS fluorescence intensity in HT-22 cells relative to the HG group (Figs. 6D and 6E). These outcomes implied that nuciferine safeguarded HT-22 cells against oxidative stress caused by HG.

### *3.7. Nuciferine conferred neuroprotection via inverting the dysregulation of the PI3K/AKT signaling pathway in HG-induced HT-22 cells*

HG significantly decreased the mRNA levels of *IGF-1R*, *IRS1*, *PI3K*, and *AKT*, while enhancing *GSK3β* mRNA expression. Nuciferine treatment effectively reversed these changes (Figs. 7A–7E). At the protein level, compared with the CON group, HG downregulated IR level, and the ratio of p-IGF-1R/IGF-1R, p-PI3K/PI3K, and p-AKT/AKT, while upregulating the ratio of p-IRS1/IRS1, GSK3β level and the ratio of p-Tau/Tau. In contrast, nuciferine treatment restored IR levels and upregulated p-IGF-1R/IGF-1R, p-PI3K/PI3K, and p-AKT/AKT ratios while downregulating the ratio of p-IRS1/IRS1, GSK3β level and the ratio of p-Tau/Tau in the Nuci group (Figs. 7F–7N). These findings suggested that nuciferine could alleviate HG-induced toxicity by restoring the PI3K/AKT signaling pathway.

### *3.8. Knockdown of IR blocked the neuroprotective effect of nuciferine through PI3K/AKT signaling pathway*

To identify the potential targets of nuciferine in activating the PI3K/AKT signaling pathway. Molecular docking revealed that nuciferine binded to the IR protein with an affinity of −8.1 kcal·mol$^{-1}$ and forms hydrogen bonds with ASP-1083 and LYS-1030 residues (Fig. 8A). CETSA experiments further confirmed that nuciferine enhanceed the thermal stability of IR protein (Figs. 8B and 8C). Then, we transfected HT-22 cells with IR siRNA, the results showed that knockdown of IR downregulated PI3K and AKT expression while upregulating GSK3β in the HG + Nuci group (Figs. 8D–8H). However, the level of p-Tau was not increased in the HG group after IR knockdown, possibly due to the regulation of other kinases besides GSK3β (Figs. 8D amd 8I). In addition, we used IR inhibitor (BMS-754807) and PI3K inhibitor (LY294002) to confirm that nuciferine regulates *via* the PI3K/AKT signaling pathway. In the HG group, GSK3β and p-Tau/Tau levels increased but reversed upon nuciferine treatment. However, adding BMS-754807 and LY294002 inhibited nuciferine's effects on GSK3β and p-Tau/Tau expression (Fig. S6). These findings indicated that nuciferine exerted neuroprotective effects by targeting IR to activate PI3K/AKT signaling pathway.

## 4. Discussion

Nuciferine is a key quality indicator and primary active com-

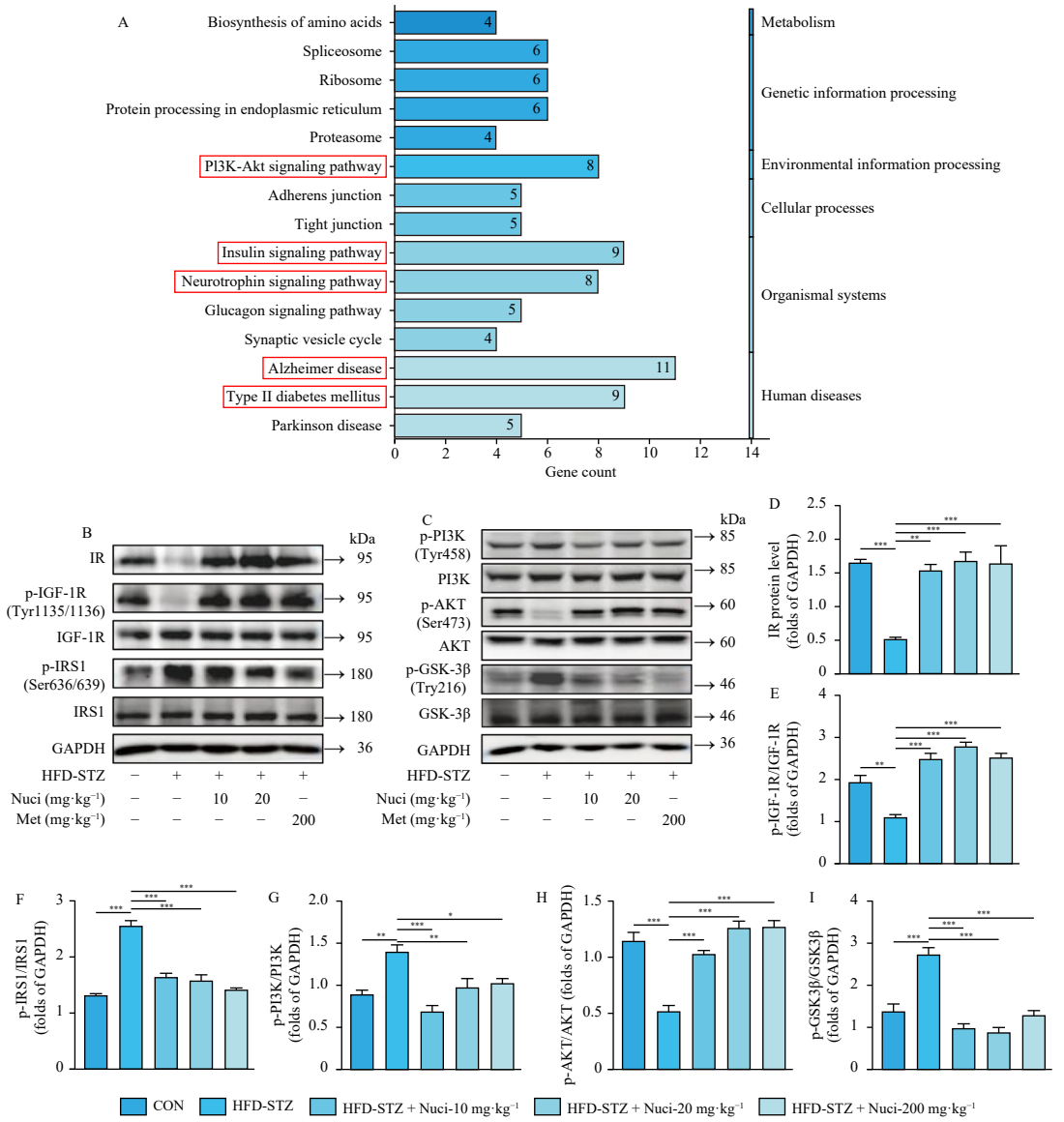



**Fig. 5** The PI3K/AKT signaling pathway played a critical role in the effect of nuciferine on cognitive impairment in HFD/STZ-induced mice. The differential proteins of mice hippocampal tissue after treatment with nuciferine were analyzed by proteomics. (A) KEGG pathway enrichment analysis of differential proteins in the hippocampus of mice between nuciferine and HFD/STZ group. (B and C) Representative Western blot analysis was conducted for IR, p-IGF-1R/IGF-1R, p-IRS1/IRS1, p-PI3K/PI3K, p-AKT/AKT, and GSK3β in the hippocampus. Quantitative analysis of the blot intensity for IR (D) and the ratios of p-IGF-1R/IGF-1R (E), p-IRS1/IRS1 (F) as presented in (B). Quantitative analysis of the blot intensity for the ratios of p-PI3K/PI3K (G), p-AKT/AKT (H), and GSK3β (I) as shown in (C). Data were expressed as mean ± SEM ($n$ = 3). $^{*}P < 0.05$, $^{**}P < 0.01$, $^{***}P < 0.001$.

ponent of lotus leaves [24]. The *Chinese Pharmacopoeia* classified lotus leaf as a food-medicine substance. In TCM, it is characterized as bitter-astringent and neutral, associated with the liver, spleen, stomach, and heart meridians [25]. Clinical studies have shown that the TCM containing nuciferine have therapeutic effects in the treatment, including hyperglycemia, diabetes mellitus and chronic intestinal inflammation [26]. Researchers [27, 28] employed the LC-MS/MS content determination method to investigate the pharmacokinetic characteristics of nuciferine at different oral doses in the plasma of SD rats. The absolute bioavailability of nuciferine in the body was low and dose-independent. The concentration of nuciferine in brain tissue was nearly equivalent to that in the plasma, suggesting that nuciferine can penetrate the blood-brain barrier. Oral administration of nuciferine at doses of 10 and 15 $mg \cdot kg^{-1}$ significantly decreased the expression of lipolysis and the secretion of very low-density lipoprotein related to a gene in hamsters induced by a HFD [29]. When nuciferine was orally administered at 0.06% and 0.12% *W/W*, the hepatic levels of triglyceride and low-density lipoprotein cholesterol were reduced. Specifically, they were approximately 55% and 40% lower respectively compared to those in HFD/STZ-induced T2DMmice [30]. In gestational diabetes mellitus mice, nuciferine can reduce lipid accumulation in the liver and increase the contents of hepatic glycogen and placental glycogen [31].Therefore, oral administration of nuciferine has hypoglycemic effects and can pass through the BBB.

T2DM-CI is a chronic complication of T2DM with complex pathogenesis. Single-target chemical drugs frequently exhibit limitations, including inadequate safety, restricted functionality, and suboptimal efficacy. Consequently, developing multi-target drugs from natural resources is essential for managing T2DM-CI. In this study, the therapeutic effects and underlying mechanisms of nuciferine in mitigating on T2DM-CI were comprehensively validated through *in vivo* experiments using HFD/STZ and ICV/STZ mouse models, as well as *in vitro* experiment using HG-induced HT-22 cell model. The combination of HFD and multiple low-dose intraperitoneal STZ injections partially impairs *β*-cell function, mimicking the insulin secretion defect and hyperglycemia of T2DM, and indirectly damages hippocampal neurons and cognitive function [32]. This combined induction method has certain ad-

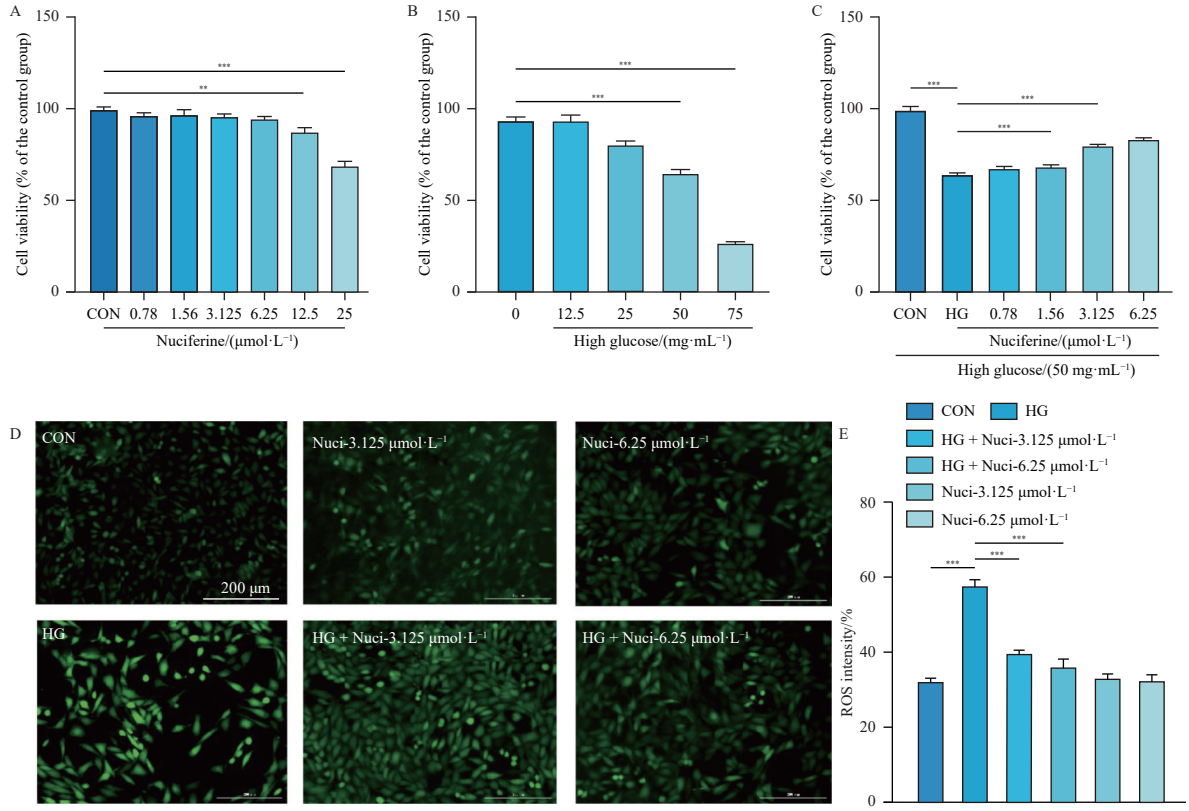
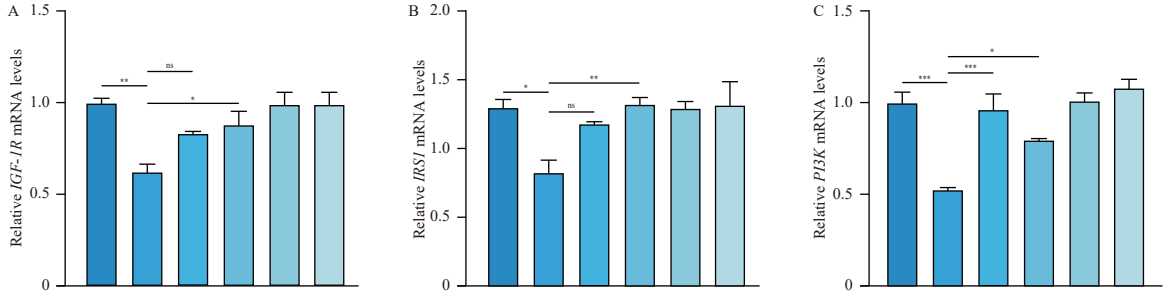



**Fig. 6** Nuciferine alleviated the toxicity and ROS generation in HG induced- HT-22 cells. (A) The cell viability were exposed to 0.78–25 μmol·L$^{-1}$ nuciferine or (B) HG (12.5–75 mg·mL$^{-1}$) assessed separately by the MTT assay in HT-22 cells. (C) HT-22 cells were pretreated with nuciferine (0.78–6.25 μmol·L$^{-1}$) for 4 h, and then exposed to HG (50 mg·mL$^{-1}$) for 24 h. The cell viability were detected by the MTT assay ($n$ = 4–5). (D) The effect of nuciferine on the ROS levels in HT-22 cells was determined by a DCF-DA fluorescent probe. (E) Quantitative assessment of ROS generation ($n$ = 3). Data were expressed as mean ± SEM. $^{**}P < 0.01$, $^{***}P < 0.001$.

vantages in simulating hyperglycemia and insulin resistance, but its main limitation lies in the fact that it cannot fully replicate the natural course of human diabetes. There are differences in pathological mechanisms and complications [33]. But a recent study has also pointed out that [34] the combination of a HFD and the administration of 200 mg·kg$^{-1}$ STZ *via* a micro-pump has established a reproducible *in vivo* mouse model of T2D, which replicates several key pathophysiological changes seen in human T2D patients. And intracerebroventricular injection of STZ directly disrupts central insulin signal transduction [35], leading to decreased synaptic plasticity, excessive phosphorylation of Tau protein, thereby simulating AD-like pathology [36]. Both insulin resistance and cognitive impairment are observed in these two models. In this study, we established two mouse models, HFD-STZ and ICV-STZ, to investigate the protective effects of nuciferine. Metformin is the most commonly used oral hypoglycemic drug for T2DM, enhancing insulin sensitivity and glucose uptake [37]. It also slows neurodegeneration and reduces T2DM-related cognitive dysfunction [38-40]. Due to its effects on peripheral insulin resistance and neuroprotection, metformin served as the positive control in the HFD-STZ mouse model. Donepezil, an acetylcholinesterase (AChE) inhibitor effective for mild to moderate cognitive impairmen [41], was used as the positive control in the ICV-STZ model. Results showed that HFD-STZ mice exhibited weight loss, elevated blood glucose levels and impaired glucose tolerance. After nuciferine intervention, their weight stabilized, blood glucose significantly decreased and improved glucose tolerance. MWM and NOR tests revealed learning and memory deficits in both model groups, which were ameliorated after nuciferine treatment, as evidenced by shorter escape latency, increased platform crossings, and enhanced DI. HE staining showed that nuciferine increased the neuronal survival in model mice. Immunofluorescence analysis demonstrated nuciferine restored synaptic injury and reduced glial cell activation. Western blot and immunofluorescence showed elevated Tau and p-Tau protein levels in model mice, which were reduced by nuciferine. Thus, these findings indicated that nuciferine exerted protective effects against T2DM-CI by ameliorating insulin resistance, regulating blood glucose levels, enhancing cognitive function, reducing inflammatory response, attenuating hippocampal damage and Tau protein phosphorylation.

To further investigate the mechanisms underlying nuciferine's amelioration of T2DM-CI, we performed proteomic analysis on mouse hippocampal tissues. 158 differentially expressed pro-



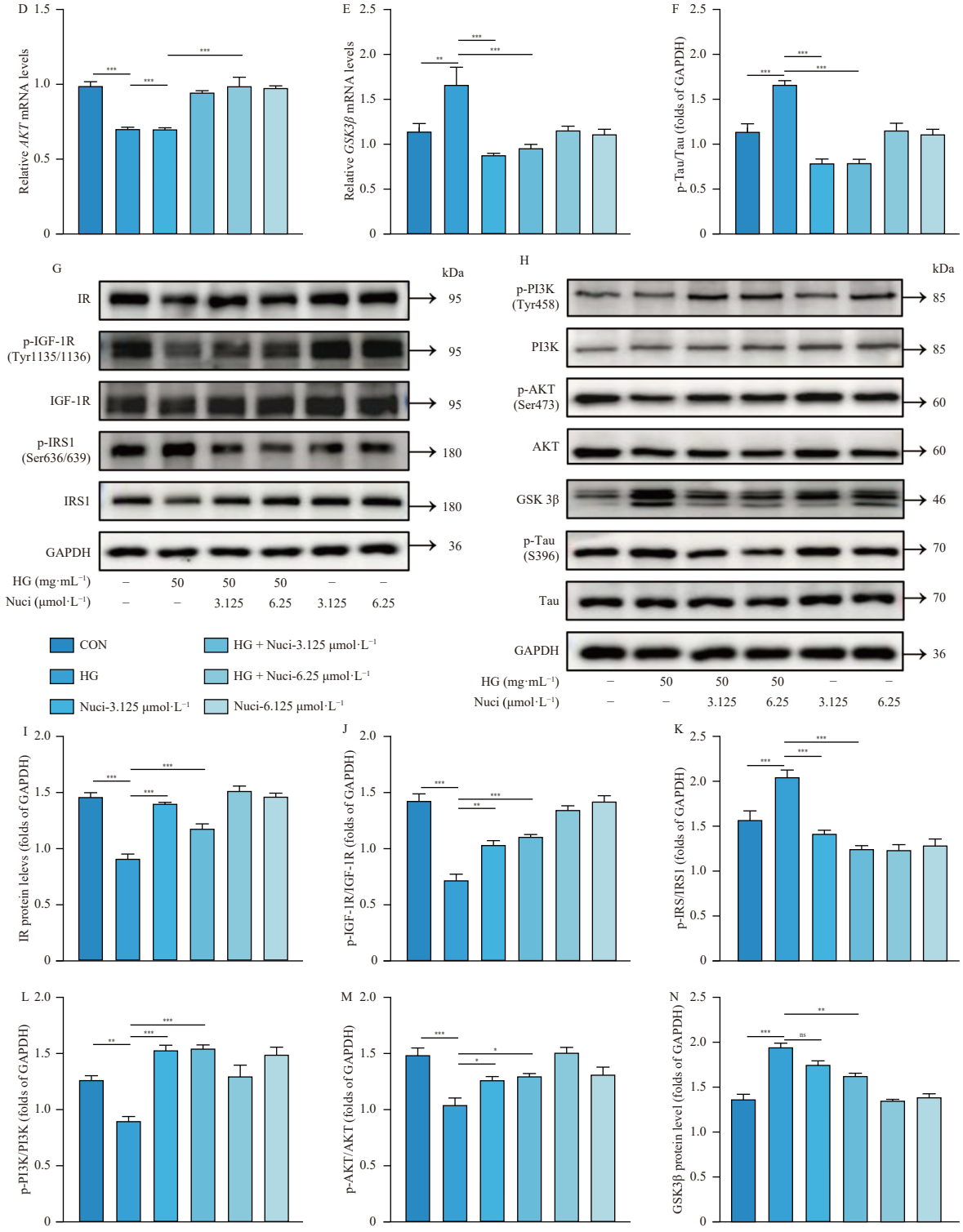



**Fig. 7** Nuciferine provided neuroprotection by reversing the dysregulation of the PI3K/AKT signaling pathway in HG-induced HT-22 cells. (A–E) The mRNA levels of *IGF-1R*, *IRS1*, *PI3K*, *AKT*, and *GSK3β* were detected by RT-qPCR analysis in HT-22 cells. (G and H) IR, p-IGF-1R, IGF-1R, p-IRS1, IRS1, p-PI3K, PI3K, p-AKT, AKT, GSK3β, p-Tau and Tau were detected by Western blot analysis in HT-22 cells. Quantitative analysis of IR (I) and the ratios of p-IGF-1R/IGF-1R (J) as well as p-IRS1/IRS1 (K) in panel (G). Quantitative analysis for the ratios of p-PI3K/PI3K (L) , p-AKT/AKT (M), as well as GSK3β (N), and the ratio of p-Tau/Tau (F) in panel (H). Data were expressed as mean ± SEM ($n$ = 3). $^{*}P < 0.05$, $^{**}P < 0.01$, $^{***}P < 0.001$; ns: no significance.

teins between the nuciferine and model groups were identified. GO analysis and KEGG analysis revealed the connection between insulin resistance and cognitive impairment, and the PI3K/AKT signaling pathway was significantly enriched, indicating its potential as a critical target for nuciferine to improve T2DM-CI. The PI3K/AKT signaling pathway is one of the primary pathways involved in insulin signaling. In insulin resistance, the activity of the PI3K/AKT pathway is significantly reduced [42]. Upon binding of insulin or insulin-like growth factor (IGF) to their receptors, IR and insulin-like growth factor-1 receptor (IGF-1R), tyrosine kinase is activated, leading to the phosphorylation of IRS1. Phosphorylated IRS1 regulates processes such as glucose metabolism, neuronal maturation, and synapse formation [43, 44]. As a core downstream pathway of IRS1, PI3K/AKT is activated by the phosphorylation of IRS1, and further activating AKT [45]. Activated AKT promotes glucose metabolism and stabilizing Tau protein phos-

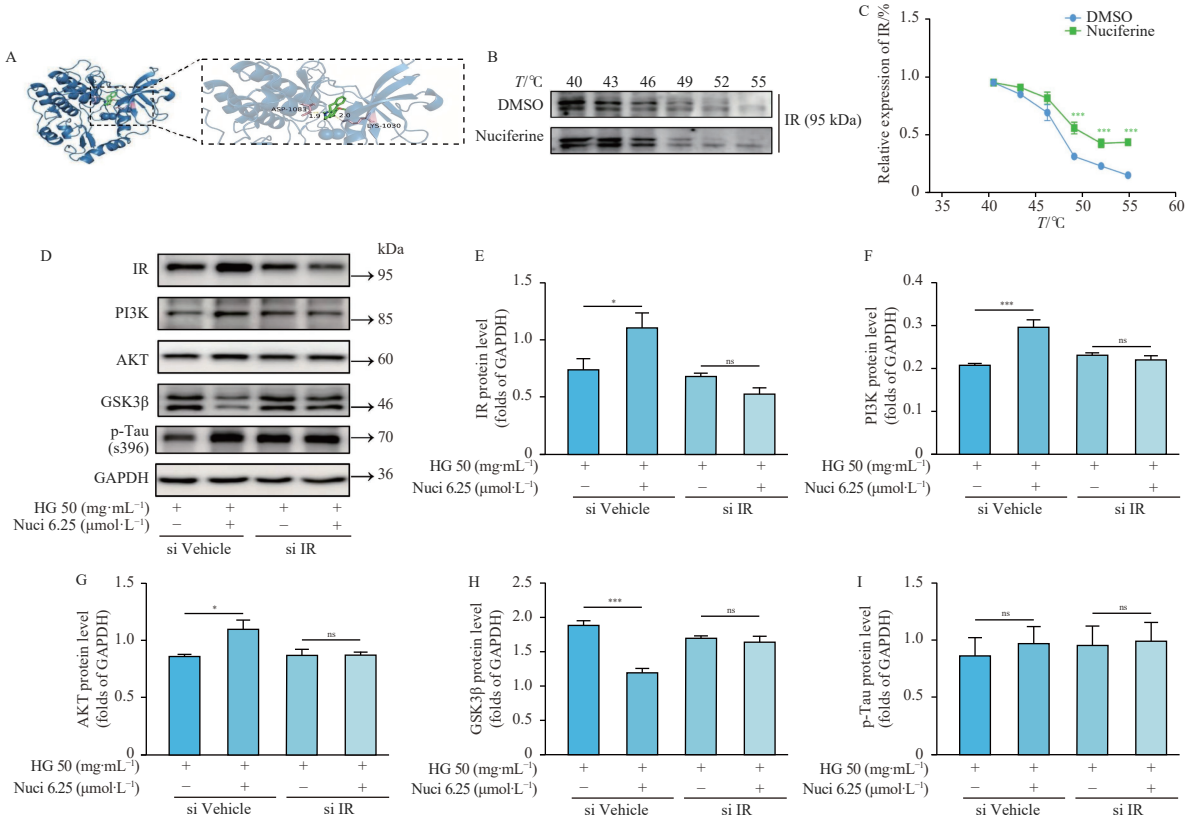



**Fig. 8** Knockdown of IR blocked the neuroprotective effect of nuciferine through PI3K/AKT signaling pathway. (A) The optimal conformation of molecular docking between nuciferine and IR (PDB ID: 3BU6). The figure in the right box is an enlarged version of the structure presented on the left. (B and C) HT-22 cells incubated with or without nuciferine (25 μmol·L$^{-1}$) for 4 h were subjected to CETSA assay. (D) Western blot analysis was employed to detect IR and its downstream major targets PI3K/AKT/GSK3β and p-Tau in HT-22 cells treated with IR-siRNA or vehicle-siRNA. Quantitative analysis of IR (E), PI3K (F), AKT (G), GSK3β (H), and p-Tau (I) is presented as shown in (D). Data were expressed as mean ± SEM ($n$ = 3). $^{*}P < 0.05$, $^{***}P < 0.001$, and ns: no significance.

phorylation by inhibiting GSK3β activity [46]. Previous studies have demonstrated that the PI3K/AKT signaling pathway is involved in the pathological process of AD by regulating the phosphorylation of Tau protein and reducing the deposition ofAβ [47-49]. Besides, some studies collectively indicate the therapeutic potential of natural compounds in ameliorating AD by targeting the PI3K/AKT signaling pathway and addressing insulin resistance [36, 50, 51].

The present study confirmed that nuciferine improved cognitive function and insulin resistance *via* modulation of the IR/IRS1/PI3K/AKT/GSK3β signaling pathway in the HFD-STZ model or ICV-STZ model. In HT-22 cell model, nuciferine mitigated HG-induced reductions in cell viability. Furthermore, nuciferine reduced oxidative stress, Tau phosphorylation and alleviated cognitive impairment through modulation of the PI3K/AKT pathway at both gene and protein levels. To investigate the potential targets of nuciferine in activating the PI3K/AKT signaling pathway, we utilized the PDBbind+ database and identified the IR protein as a key target. Molecular docking (binding energy: −8.1 kcal·mol$^{-1}$) and CETSA confirmed the excellent binding activity of nuciferine with IR protein. Besides, after IR was knocked down in HT-22 cells, the down-regulation of PI3K and AKT expression and the up-regulation of GSK3β expression induced by HG could not be reversed by nuciferine. IR inhibitor (BMS-754807) and PI3K inhibitor (LY294002) also blocked nuciferine-mediated regulation of the PI3K/AKT signaling pathway.

Most existing studies have focused separately on the metabolic or neurological effects of nuciferine, without integrating both aspects or identifying its specific target and mechanism in T2DM-CI. This study's innovation is mainly reflected in two aspects: first, nuciferine directly binds to IR and acts through this key target, filling a gap in its mechanism within the insulin signaling pathway. Second, by simultaneously using HFD-STZ (modeling peripheral insulin resistance and hyperglycemia-induced T2DM-CI) and ICV-STZ (modeling central insulin signaling defects) animal models, along with a HG-induced HT-22 cell model, the therapeutic effects of nuciferine on T2DM-CI were validated across *in vivo* and *in vitro*, overcoming the limitations of single-model studies and enhancing the comprehensiveness and reliability of the findings. Based on the finding that nuciferine improves cognition in the ICV-STZ model (without peripheral hyperglycemia), its glucose-independent neuroprotective effects were investigated, including direct inhibition of neuroinflammation (reducing activation of Iba1$^{+}$ microglia and GFAP$^{+}$ astrocytes), suppression of Tau hyperphosphorylation (*via* the IR/PI3K/AKT/GSK3β pathway). These effects are independent of glucose regulation and reflect a direct neuroprotective mechanism through which nuciferine exerts its therapeutic effects on cognitive impairment.

In addition, nuciferine reduces Tau phosphorylation by inhibiting GSK3β activity and up-regulating the expression of Aβ-degrading enzymes (IDE, NEP). In light of the core pathological features of abnormal Tau and Aβ deposition in the brains of AD patients, we will further study the role of nuciferine in regulating Tau and Aβ metabolism in AD transgenic animal models.

## 5. Conclusion

In conclusion, these experimental findings indicate that nuciferine activates the PI3K/AKT signaling pathway by targeting IR, thereby improving insulin resistance and attenuating the progression of T2DM-CI (Fig. 9).

## Supporting information

Supporting information of this paper can be requested by

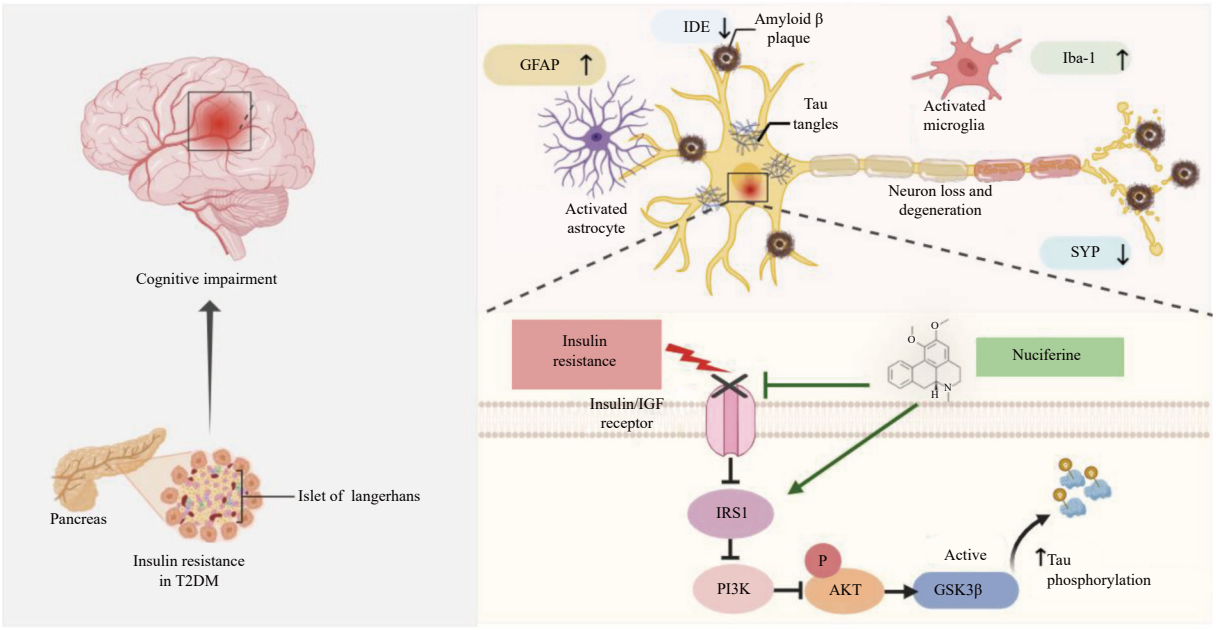



**Fig. 9** The mechanism diagram of nuciferine in ameliorating T2DM-induced cognitive impairment. Insulin resistance in brain is an important factor in inducing cognitive impairment. Nuciferine acts directly on IR, activates P13K/AKT pathway, inhibits GSK3β activity, reduces the production of phosphorylated Tau protein, inhibites glial cell activation, promotes neuronal survival, increases the synaptic proteins levels, improves insulin resistance, and cognitive impairment.

sending E-mail to the corresponding author.

## Declaration of competing interest

All authors disclosed no relevant relationships.

## Acknowledge

The authors acknowledge the support from the Scientific Research Center, Hangzhou Medical College.

## References

1 Mancusi C, Izzo R, Di Gioia G, et al. Insulin resistance the hinge between hypertension and type 2 diabetes. *High Blood Press Cardiovasc Prev*. 2020;27(6):515-526. https://doi.org/10.1007/s40292-020-00408-8.
2 Jensen TS, Karlsson P, Gylfadottir SS, et al. Painful and non-painful diabetic neuropathy, diagnostic challenges and implications for future management. *Brain*. 2021;144(6):1632-1645. https://doi.org/10.1093/brain/awab079.
3 Fung TH, Patel B, Wilmot EG, et al. Diabetic retinopathy for the non-ophthalmologist. *Clin Med (Lond)*. 2022;22(2):112-116. https://doi.org/10.7861/clinmed.2021-0792.
4 Deng L, Yang Y, Xu G. Empagliflozin ameliorates type 2 diabetes mellitus-related diabetic nephropathy *via* altering the gut microbiota. *Biochim Biophys Acta Mol Cell Biol Lipids*. 2022;1867(12):159234. https://doi.org/10.1016/j.bbalip.2022.159234.
5 Karabaeva RZ, Vochshenkova TA, Mussin NM, et al. Epigenetics of hypertension as a risk factor for the development of coronary artery disease in type 2 diabetes mellitus. *Front Endocrinol (Lausanne)*. 2024;15:1365738. https://doi.org/10.3389/fendo.2024.1365738.
6 Li C, Bishop TRP, Imamura F, et al. Meat consumption and incident type 2 diabetes: an individual-participant federated meta-analysis of 1.97 million adults with 100 000 incident cases from 31 cohorts in 20 countries. *Lancet Diabetes Endocrinol*. 2024;12(9):619-630. https://doi.org/10.1016/S2213-8587(24)00179-7.
7 Busche MA, Hyman BT. Synergy between amyloid-β and tau in Alzheimer's disease. *Nat Neurosci*. 2020;23(10):1183-1193. https://doi.org/10.1038/s41593-020-0687-6.
8 2023 Alzheimer's disease facts and figures. *Alzheimers Dement*. 2023;19(4):1598-1695. https://doi.org/10.1002/alz.13016.
9 Van Gennip ACE, Stehouwer CDA, Van Boxtel MPJ, et al. Association of type 2 diabetes, according to the number of risk factors within target range, with structural brain abnormalities, cognitive performance, and risk of dementia. *Diabetes Care*. 2021;44(11):2493-2502. https://doi.org/10.2337/dc21-0149.
10 Rezaei MH, Madadizadeh E, Aminaei M, et al. Leptin signaling could mediate hippocampal decumulation of *β*-amyloid and Tau induced by high-intensity interval training in rats with type 2 diabetes. *Cell Mol Neurobiol*. 2023;43(7):3465-3478. https://doi.org/10.1007/s10571-023-01357-1.
11 Pignalosa FC, Desiderio A, Mirra P, et al. Diabetes and cognitive impairment: a role for glucotoxicity and dopaminergic dysfunction. *Int J Mol Sci*. 2021;22(22):12366. https://doi.org/10.3390/ijms222212366.
12 Akhtar A, Sah SP. Insulin signaling pathway and related molecules: role in neurodegeneration and Alzheimer's disease. *Neurochem Int*. 2020;135:104707. https://doi.org/10.1016/j.neuint.2020.104707.
13 Gupta S, Singh V, Ganesh S, et al. siRNA mediated GSK3β knockdown targets insulin signaling pathway and rescues Alzheimer's disease pathology: evidence from *in vitro* and *in vivo* studies. *ACS Appl Mater Interfaces*. 2022;14(1):69-93. https://doi.org/10.1021/acsami.1c15305.
14 Saltiel AR. Insulin signaling in health and disease. *J Clin Invest*. 2021;131(1):e142241. https://doi.org/10.1172/JCI142241.
15 Gabbouj S, Ryhanen S, Marttinen M, et al. Altered insulin signaling in Alzheimer's disease brain-special emphasis on PI3K-Akt pathway. *Front Neurosci*. 2019;13:629. https://doi.org/10.3389/fnins.2019.00629.
16 Sharma BR, Gautam LN, Adhikari D, et al. A comprehensive review on chemical profiling of nelumbo nucifera: potential for drug development. *Phytother Res*. 2017;31(1):3-26. https://doi.org/10.1002/ptr.5732.
17 Ren X, Chen H, Wang H, et al. Advances in the pharmacological effects and mechanisms of *Nelumbo nucifera* Gaertn extract nuciferine. *J Ethnopharmacol*. 2024;331:118262. https://doi.org/10.1016/j.jep.2024.118262.
18 Wan Y, Xia J, Xu JF, et al. Nuciferine, an active ingredient derived from lotus leaf, lights up the way for the potential treatment of obesity and obesity-related diseases. *Pharmacol Res*. 2022;175:106002. https://doi.org/10.1016/j.phrs.2021.106002.
19 Wang Y, Yao W, Li B, et al. Nuciferine modulates the gut microbiota and prevents obesity in high-fat diet-fed rats. *Exp Mol Med*. 2020;52(12):1959-1975. https://doi.org/10.1038/s12276-020-00534-2.
20 Qiu J, Le Y, Liu N, et al. Nuciferine alleviates high-fat diet- and ApoE$^{(-/-)}$-induced hepatic steatosis and ferroptosis in NAFLD mice *via* the PPARα signaling pathway. *J Agric Food Chem*. 2024;72(44):24417-24431. https://doi.org/10.1021/acs.jafc.4c04929.
21 Li J, Dong S, Quan S, et al. Nuciferine reduces inflammation induced by cerebral ischemia-reperfusion injury through the PI3K/Akt/NF-κB pathway. *Phytomedicine*. 2024;125:155312. https://doi.org/10.1016/j.phymed.2023.155312.
22 Chen C, Ma Q, Jiang J, et al. Protective effects of nuciferine in middle cerebral artery occlusion rats based on transcriptomics. *Brain Sci*. 2022;12(5):572. https://doi.org/10.3390/brainsci12050572.
23 Gao L, Wu S, Hu B, et al. Targeting the RAGE-RIPK1 binding site attenuates diabetes-associated cognitive deficits. *J Neuroinflammation*. 2025;22(1):162. https://doi.org/10.1186/s12974-025-03489-1.
24 Deng H, Xu Q, Sang XT, et al. Study on the vasodilatory activity of lotus leaf extract and its representative substance nuciferine on thoracic aorta in rats. *Front Pharmacol*. 2022;13:946445. https://doi.org/10.3389/fphar.2022.946445.
25 Xu X, Xu H, Shang Y, et al. Development of the general chapters of the *Chinese Pharmacopoeia* 2020 edition: a review. *J Pharm Anal*. 2021;11(4):398-404. https://doi.org/10.1016/j.jpha.2021.05.001.
26 Zhao T, Zhu Y, Zhao R, et al. Structure-activity relationship, bioactivities, molecular mechanisms, and clinical application of nuciferine on inflammation-related diseases. *Pharmacol Res*. 2023;193:106820. https://doi.org/10.1016/j.phrs.2023.106820.
27 Gu S, Zhu G, Wang Y, et al. A sensitive liquid chromatography-tandem mass spectrometry method for pharmacokinetics and tissue distribution of nuciferine in rats. *J Chromatogr B Analyt Technol Biomed Life Sci*. 2014;961:20-28. https://doi.org/10.1016/j.jchromb.2014.04.038.
28 Wang F, Cao J, Hou X, et al. Pharmacokinetics, tissue distribution,

bioavailability, and excretion of nuciferine, an alkaloid from lotus, in rats by LC/MS/MS. *Drug Dev Ind Pharm*. 2018;44(9):1557-1562. https://doi.org/10.1080/03639045.2018.1483399.
29 Guo F, Yang X, Li X, et al. Nuciferine prevents hepatic steatosis and injury induced by a high-fat diet in hamsters. *PLoS One*. 2013;8(5):e63770. https://doi.org/10.1371/journal.pone.0063770.
30 Zhang C, Deng J, Liu D, et al. Nuciferine ameliorates hepatic steatosis in high-fat diet/streptozocin-induced diabetic mice through a PPARα/PPARγ coactivator-1α pathway. *Br J Pharmacol*. 2018;175(22):4218-4228. https://doi.org/10.1111/bph.14482.
31 Tang Z, Luo T, Huang P, et al. Nuciferine administration in C57BL/6J mice with gestational diabetes mellitus induced by a high-fat diet: the improvement of glycolipid disorders and intestinal dysbacteriosis. *Food Funct*. 2021;12(22):11174-11189. https://doi.org/10.1039/d1fo02714j.
32 Zheng Y, Zhang J, Zhao Y, et al. Curcumin protects against cognitive impairments in a rat model of chronic cerebral hypoperfusion combined with diabetes mellitus by suppressing neuroinflammation, apoptosis, and pyroptosis. *Int Immunopharmacol*. 2021;93:107422. https://doi.org/10.1016/j.intimp.2021.107422.
33 Chandrasekera PC, Pippin JJ. Of rodents and men: species-specific glucose regulation and type 2 diabetes research. *ALTEX*. 2014;31(2):157-176. https://doi.org/10.14573/altex.1309231.
34 Attrill EH, Scharapow O, Perera S, et al. Controlled induction of type 2 diabetes in mice using high fat diet and osmotic-mini pump infused streptozotocin. *Sci Rep*. 2025;15(1):8812. https://doi.org/10.1038/s41598-025-89162-2.
35 Rostami F, Javan M, Moghimi A, et al. Prenatal stress promotes icv-STZ-induced sporadic Alzheimer's pathology through central insulin signaling change. *Life Sci*. 2020;241:117154. https://doi.org/10.1016/j.lfs.2019.117154.
36 Huang J, Xu Z, Yu C, et al. The volatile oil of *Acorus tatarinowii* Schott ameliorates Alzheimer's disease through improving insulin resistance *via* activating the PI3K/AKT pathway. *Phytomedicine*. 2024;135:156168. https://doi.org/10.1016/j.phymed.2024.156168.
37 Herman R, Kravos NA, Jensterle M, et al. Metformin and insulin resistance: a review of the underlying mechanisms behind changes in GLUT4-mediated glucose transport. *Int J Mol Sci*. 2022;23(3):1264. https://doi.org/10.3390/ijms23031264.
38 Taheri M, Roghani M, Sedaghat R. Metformin mitigates trimethyltin-induced cognition impairment and hippocampal neurodegeneration. *Cell Mol Neurobiol*. 2024;44(1):70. https://doi.org/10.1007/s10571-024-01502-4.
39 Ozbey G, Nemutlu-Samur D, Parlak H, et al. Metformin protects rotenone-induced dopaminergic neurodegeneration by reducing lipid peroxidation. *Pharmacol Rep*. 2020;72(5):1397-1406. https://doi.org/10.1007/s43440-020-00095-1.
40 Hong S, Nagayach A, Lu Y, et al. A high fat, sugar, and salt Western diet induces motor-muscular and sensory dysfunctions and neurodegeneration in mice during aging: ameliorative action of metformin. *CNS Neurosci Ther*. 2021;27(12):1458-1471. https://doi.org/10.1111/cns.13726.
41 Oliveira SR, Counil H, Rabanel JM, et al. Donepezil-loaded nanocarriers for the treatment of Alzheimer's disease: superior efficacy of extracellular vesicles over polymeric nanoparticles. *Int J Nanomed*. 2024;19:1077-1096. https://doi.org/10.2147/IJN.S449227.
42 Zheng M, Wang P. Role of insulin receptor substance-1 modulating PI3K/Akt insulin signaling pathway in Alzheimer's disease. *3 Biotech*. 2021;11(4):179. https://doi.org/10.1007/s13205-021-02738-3.
43 Rethelyi JM, Vincze K, Schall D, et al. The role of insulin/IGF1 signalling in neurodevelopmental and neuropsychiatric disorders: evidence from human neuronal cell models. *Neurosci Biobehav Rev*. 2023;153:105330. https://doi.org/10.1016/j.neubiorev.2023.105330.
44 Choi E, Duan C, Bai XC. Regulation and function of insulin and insulin-like growth factor receptor signalling. *Nat Rev Mol Cell Biol*. 2025;26(7):558-580. https://doi.org/10.1038/s41580-025-00826-3.
45 Meng Q, Qi X, Chao Y, et al. IRS1/PI3K/AKT pathway signal involved in the regulation of glycolipid metabolic abnormalities by mulberry (*Morus alba* L.) leaf extracts in 3T3-L1 adipocytes. *Chin Med*. 2020;15:1. https://doi.org/10.1186/s13020-019-0281-6.
46 Xu A, Zeng Q, Tang Y, et al. Electroacupuncture protects cognition by regulating Tau phosphorylation and glucose metabolism *via* the AKT/GSK3β signaling pathway in Alzheimer's disease model mice. *Front Neurosci*. 2020;14:585476. https://doi.org/10.3389/fnins.2020.585476.
47 Liu S, Xu L, Shen Y, et al. Qingxin Kaiqiao Fang decreases Tau hyperphosphorylation in Alzheimer's disease *via* the PI3K/Akt/GSK3β pathway *in vitro* and *in vivo*. *J Ethnopharmacol*. 2024;318(Pt B):117031. https://doi.org/10.1016/j.jep.2023.117031.
48 Peng X, Guo H, Zhang X, et al. TREM2 inhibits Tau hyperphosphorylation and neuronal apoptosis *via* the PI3K/Akt/GSK-3β signaling pathway *in vivo* and *in vitro*. *Mol Neurobiol*. 2023;60(5):2470-2485. https://doi.org/10.1007/s12035-023-03217-x.
49 Qiu Q, Lei X, Wang Y, et al. Naringin protects against Tau hyperphosphorylation in Aβ (25-35)-injured PC12 cells through modulation of ER, PI3K/AKT, and GSK-3β signaling pathways. *Behav Neurol*. 2023;2023:1857330. https://doi.org/10.1155/2023/1857330.
50 Zhang W, Zhang Z, Xiang Y, et al. Aurora kinase A-mediated phosphorylation triggers structural alteration of Rab1A to enhance ER complexity during mitosis. *Nat Struct Mol Biol*. 2024;31(2):219-231. https://doi.org/10.1038/s41594-023-01165-7.
51 Xiong R, Wang XL, Wu JM, et al. Polyphenols isolated from lychee seed inhibit Alzheimer's disease-associated Tau through improving insulin resistance *via* the IRS-1/PI3K/Akt/GSK-3β pathway. *J Ethnopharmacol*. 2020;251:112548. https://doi.org/10.1016/j.jep.2020.112548.